



# Performance Analysis and Characterization of Natural Dye-sensitized Solar Cells (DSSCs) of Titanium Oxide (TiO<sub>2</sub>) Thin Film

Ngozi loveth Arinze-Umobi <sup>a\*</sup>, Nwokoye Anthony <sup>a</sup>,  
Azubike Josiah Ekpunobi <sup>a</sup>  
and Okafor Chiedozie Emmanuel <sup>a</sup>

<sup>a</sup> Department of Physics and Industrial Physics, Faculty of Physical Science, Nnamdi Azikiwe University Awka, Anambra State, Nigeria.

## Authors' contributions

This work was carried out in collaboration among all authors. All authors read and approved the final manuscript.

## Article Information

DOI: <https://doi.org/10.9734/ajopacs/2024/v12i4235>

## Open Peer Review History:

This journal follows the Advanced Open Peer Review policy. Identity of the Reviewers, Editor(s) and additional Reviewers, peer review comments, different versions of the manuscript, comments of the editors, etc are available here: <https://www.sdiarticle5.com/review-history/127155>

Original Research Article

Received: 25/09/2024

Accepted: 27/11/2024

Published: 09/12/2024

## ABSTRACT

Dye-sensitized solar cells (DSSCs) thin films of titanium oxide (TiO<sub>2</sub>) sensitized with the dyes of the almond and copper leaves extracted using ethanol and water (AE, AW, CE and CW) each, have been successfully deposited on FTO conductive glass substrate using the Dr Blading method. The deposited TiO<sub>2</sub>-DSSC thin films were subjected to UV-Vis spectroscopy, X-ray diffraction, scanning electron microscopy and I-V characteristics analysis to determine their optical, structural,

\*Corresponding author: E-mail: lovethumobi@gmail.com;

morphological properties and solar cell parameters respectively. The results of the analysis showed that copper leaves dye-sensitized films (CE and CW) has absorbance is in the range of 0.45 to 0.9 and 0.25 to 0.45 respectively within the visible (VIS) regions. The absorbance of the films sensitized with almond leaves dye is lower in the range of 0.15 - 0.25 for AE and 0.04 – 0.09 for AW within the region. The percentage transmittance of the films was found to be in the range of 82.5% – 90% for the film AW, 35% – 55% for CW while the film AE has the lowest value of the order 12.5% - 35% within the VIS region. The reflectance percent of the films were generally low with the film CE having the highest value in the range of 27%-43%, CW in the range 17.5% - 26%, AE in the range 10% - 15%, while the film AW has values in the range 2.5% - 5.5% within the VIS region. All the deposited DSSCs films have high refractive index values throughout the VIS region. The bandgap energy values obtained for the films are 2.5 eV for film CE, 2.6 eV for CW, and 2.4 eV for the films AE and AW each. These are in the range of wide bandgap energies and are favourable for application in the device that required high temperature and fabrication of blue LEDs. The results of the structural analysis on the deposited thin films showed that both the films exhibited crystalline structure with crystallite sizes of 24.55 nm for CE, 27.68 nm for CW, 22.27 for AE and 36.30 for AW films. The films have low cell conversion efficiency but still within the margin of error for most DSSCs materials.

*Keywords: Titanium oxide; almond leaves; copper leaves; DSSCs; bandgap; cell-efficiency; XRD.*

## 1. INTRODUCTION

The harmful effects associated with the use of fossil fuels has been attributed to the world's heavily energy consumption reliance on fossil energy sources, (Nwokoye & Okoye, 2020). This trend has resulted in environmental pollution and prompted researchers to explore alternative energy sources. The depletion of fossil fuels energy source as they are non-renewable has also raised significant global concern due to their inability to be replenished. While numerous forms of sustainable energy technology have been developed in recent years, photovoltaic (PV) technology utilizing solar energy is widely recognized as the favourable alternative. The solar radiation from the sun amounts to about  $3 \times 10^{24}$  J per year, which is ten times the world's energy demand, (Millington, 2009) and record efficiency of 6% has been achieved since the first practical photovoltaic cell was designed in 1954 at Bell Laboratories using diffused silicon p-n junction technology, (Tsokos, 2008). Although the light to electricity conversion efficiency of silicon-based solar cells has hit up to 15% to 20%, the reliance on highly purified silicon, use of toxic chemicals in their manufacture, and high costs have generated great concern hence prompting researchers to seek for cost-effective alternatives, (Grant et al., 2002). As a result, emerging solar technology, particularly dye sensitized solar cells, has gained attention due to their promising features. Reports have suggested that the efficiency of dye molecules could be enhanced by fine-tuning the porosity of their semiconductor oxide material,

though the stability of the dye remains a significant challenge in dye-sensitized photocells. The first dye-sensitized solar cell (DSSCs) with a record design efficiency of 7.1% to 7.9% using dye sensitization on  $\text{TiO}_2$  semiconductor has been reported by O'regan & Grätzel (1991). Solar radiation can be effectively captured and converted into electricity by utilizing DSSCs technology in conjunction with natural dye as photosensitizers. In so doing, DSSCs serve as an efficient light harvesting channel due to the combination of a dye with moderate extinction and a photo anode of high surface area (approximately 1200 times the area of a flat electrode). The electrical performance of solar cells is assessed using various parameters including current density, open circuit voltage, fill factor (FF), and energy conversion efficiency. Hence the performance of DSSCs is highly dependent on the type of dye utilized as sensitizers, (Mehmood et al., 2016). The widely used industrial dye have been noted to be ruthenium (Ru) complexes. However, Ru is constrained by its high cost, scarcity and complexity of synthesis in comparison to the naturally occurring dyes derived from flowers, leaves, and fruits of plants which are cost-effective, environmentally friendly and highly abundant in nature, (Zhang et al., 2009). DSSCs can be assembled at only one-third of the cost of traditional silicon-based solar cells through a simple manufacturing process and can comprised of nano-crystalline metal oxide semiconductor layer primarily  $\text{TiO}_2$  in addition to  $\text{ZnO}$ ,  $\text{SnO}_2$ , or  $\text{NbO}_5$  that are also used, (EI-

ghamrii et al., 2014; Chou et al., 2007). In DSSCs, the dye serving as sensitizer plays a crucial role in determining the cell's efficiency by its capacity to absorb photons of visible light as the dye is primarily employed to absorb more photons corresponding to the wavelength of colour, (Tennakone et al., 1995). The DSSCs has a record efficiency of 11.20% at 1 sun when utilizing ruthenium (II) photosensitizer, (Mehmood et al., 2014). However, the commercialization of Ru-complex dye is limited by its high cost, intricate synthetic processes and susceptibility to degradation in the presence of water, hence, poses a significant environmental and health risks, (Qin & Peng, 2012). The ruthenium dye complexes contain plant pigments such as anthocyanin, carotenoid, flavonoid and chlorophyll, which are responsible for absorbing the photon energy and injecting charges into the conduction band of  $\text{TiO}_2$  by the dye sensitizer; a role that can be fulfilled by naturally occurring dyes that can be extracted from various natural sources such as flowers, fruits, leaves, seeds, barks, etc thereby cutting the cost of utilizing ruthenium dyes as well as maintaining pollution free environment. In this work, the dyes of the almond and copper leaves extracted using ethanol and water each were utilized to prepare DSSCs thin films of Titanium oxide ( $\text{TiO}_2$ ) using the Dr. Blading method to

investigate their properties for device applications.

## 2. MATERIALS AND METHODS

The following materials were used in the fabrication of the dye sensitized solar cell; Almond leaf (*terminali catappa*), copper leaf (*acalypha wilkesiana*), ethanol, titanium dioxide (Degussa P25), distilled water, filter paper, glass road, petri dish, scotch tape, aluminium foil, nose mask, mortar and pestle, lab coat, sieve, beaker, latex hand glove, digital weighing balance, oven, blender, detergent, ultra-sonicator (model: JL- 60TH). In preparation of the natural dye solutions (extracts), some quantities of the almond leaves and copper leaves were harvested from the trees, washed with regular water, and then rinsed with distilled water. The leaves were left to dry in air for four days before being processed into a powdered form. 10 g of almond leaf and copper leaf each was mixed with 100 ml of ethanol in a glass beaker and allowed to extract for one hour while covered with aluminium foil to prevent evaporation and impurities. The residues were then filtered out, and the resulting filtrates were used as photosensitizers. The same procedure was repeated using water as the extraction agent as shown in Fig. 1.



Fig. 1. Preparation of the almond and copper leaf dyes

The Fluorine-doped tin oxide (FTO) glass (resistivity 16.6  $\Omega$ /sq and thickness 3 mm) used in the fabrication of the DSSCs films was subjected to ultrasonication for 30 minutes using ethanol and another 30 minutes using distilled water to get rid of impurities. The FTO substrate was thereafter dried under compressed hot air for 30 minutes at 400°C using a furnace subject to identification of the conductive side using a digital multi-meter (DT830D). The TiO<sub>2</sub> paste was prepared by placing 1.0 g of TiO<sub>2</sub> powder (Degussa P25) in a plastic mortar and gradually adding 20 ml of methanol. This mixture was thoroughly stirred for 30 minutes with a pestle to form a homogeneous suspension. 1.0 ml of methanol was then added and the mixture was grinded before adding another 1.0 ml of the solution. This process was repeated until the entire 20 ml of methanol solution was used up taking 30 minutes in total. The homogeneous TiO<sub>2</sub> mixture was applied to the transparent FTO conducting glass, which had an average dimension of 2.35 cm by 2.50 cm, using the Dr. Blading method. By this method, two parallel edges of the conducting face of all the FTO substrates were covered with scotch tape, creating a non-coated area for electrical contact, spanning about 0.15 to 0.2 cm on the FTO substrate. With the conducting side facing upwards, a few drops of the TiO<sub>2</sub> solution were evenly distributed on the substrate, and a glass

stirring rod was used to uniformly spread the material across the FTO glass, sliding over the uncovered portion. After deposition, all the samples were allowed to dry at room temperature for 40 minutes. Subsequently, the scotch tape was carefully removed, and the electrode was sintered at 400°C for 30 minutes using a temperature-controlled furnace. The sintered TiO<sub>2</sub>-coated conductive glass substrate was gradually cooled inside the furnace to prevent cracking. These procedures were carried out to improve electrical contact and mechanical adhesion on the glass. The dyes were poured into separate beakers, and each working electrode was immersed in the respective dye solution. All the working electrodes were positioned face up inside the beakers to prevent scratching of the deposited TiO<sub>2</sub> surface. The impregnation process lasted for 24 hours to allow the dye molecules to naturally adsorb onto the TiO<sub>2</sub> particles. To prevent dye impregnation around the conducting edges of the working electrode, scotch tape was once again applied to the two parallel edges of the conducting side of all the working electrodes. Each beaker containing the samples was sealed with aluminium foil. Subsequently, the dye-stained TiO<sub>2</sub> film was carefully removed after 24 hours using tongs, and the samples were placed inside a petri dish with the sensitized surface facing up as displayed in Fig. 2.



**Fig. 2. Pictures of (a), (b) Dye sensitized films, (c) Sintered substrates immersed in the dye sensitizers covered with aluminium foil.**

In fabrication of the overall cell, a counter electrode was made from another FTO glass substrate by using lead pencil to coat the entire conductive face thus eliminating the need for scotch tape on the two parallel edges of the electrodes. A liquid electrolyte solution was prepared by dissolving 0.05 M iodide ( $I_2$ ) into acetonitrile and 0.5 M potassium iodide salt (KI). The dye-sensitized  $TiO_2$  electrode sample, with the deposited film side facing up, was placed on the table. The counter electrode was positioned on top of the sample to ensure direct contact between the conductive side of the counter electrode and that of the working electrode. The two opposing glass slides were intentionally offset so that the entire area of the working electrode was covered by the counter electrode, leaving about 0.25 cm space from the two parallel edges of the uncoated part of the glass exposed. Crocodile clips were utilized to secure the two parallel edges of the glass slides, and the liquid iodide redox electrolyte was introduced through the edges of the slides to establish a complete dye-sensitized solar cell.

The fabricated DSSCs films were subjected for optical and structural characterisation using spectrophotometry and X-ray diffraction techniques respectively to determine their properties for applications.

### 3. RESULTS AND DISCUSSION

#### 3.1 Optical properties of the Fabricated DSSCs

The optical analysis of the fabricated cells reveals how the fabricated cells interact with light which is important in understanding their behaviour for applications. Other optical properties of the deposited films were calculated from the measured absorbance values in the wavelength range of 350 nm- 800 nm. In the analysis of these properties, the deposited almond leaf dyes in water is represented with AW, almond leaf in ethanol with AE, copper leave in water with CW and copper leave in ethanol as CE.

Fig. 3 represents the graph of the measured absorbance of the deposited DSSCs films against wavelength. The figure showed that all the dye-sensitized films have peak absorbance values at 365.77 nm for CE, 368.16 nm for AE, 370.70 nm for AW and 368.16 nm for CW within the visible region of electromagnetic spectrum.

The absorbance of all the films however decreased with an increase in wavelength thus indicating lower values towards the near infrared (NIR) region. The samples CE and CW have good absorbance values in the range of 0.45 to 0.9 and 0.25 to 0.45 within the visible regions respectively. The samples AE and AW have low absorbance in the range of 0.15-0.25 and of the order 0.04 – 0.09 respectively within the VIS region. The high absorbance value of the sample CE in the VIS region showed that the deposited DSSCs films is a good absorber for solar cell fabrication.

Fig. 4 is the graph of percentage transmittance of the deposited DSSCs films as a function of wavelength to determine the transmittance characteristics of the films across the wavelength of interest. The transmittance of the films was evaluated based on the measured absorbance values using the relation as given by Nwori et al (2022).

$$T = 10^{-A} \quad 1$$

Where A is the measured absorbance of the films.

The figure indicates that the transmittance of all the dye-sensitized films increased with wavelength thus suggesting a higher transmittance in the NIR region. The film AW has the highest percentage transmittance in the range 82.5% – 90%, while the film AE has the transmittance in the range of 55% - 70%. The sample CW has transmittance range of 35% – 55% while the film CE has the lowest transmittance in the range of 12.5% - 35% within the VIS region. The increase in the percentage transmittance of the films towards the NIR region position the films for poultry house coating and for window coating in the low temperate regions of the world, (Okereke & Ekpunobi, 2011).

The graph of percentage reflectance of the deposited DSSCs thin films is displayed in figure 5. This other property was also calculated based on absorbance values using the formula provided by Ezenwaka (et al., 2022).

$$R = 1 - \sqrt{\frac{e^A}{10^A}} \quad 2$$

From the figure, it can be observed that the reflectance of the films is generally low and decreased with an increase in wavelength. The film CE has the highest reflectance range of

27%-43% within the VIS region, CW has the value in the range 17.5% - 26%, the film AE has value in the range 10% - 15%, while the film AW has the lowest reflectance value in the range

2.5% - 5.5% within the VIS region. The low reflectance values exhibited by the deposited DSSCs films make them good materials for anti-reflection coating applications.

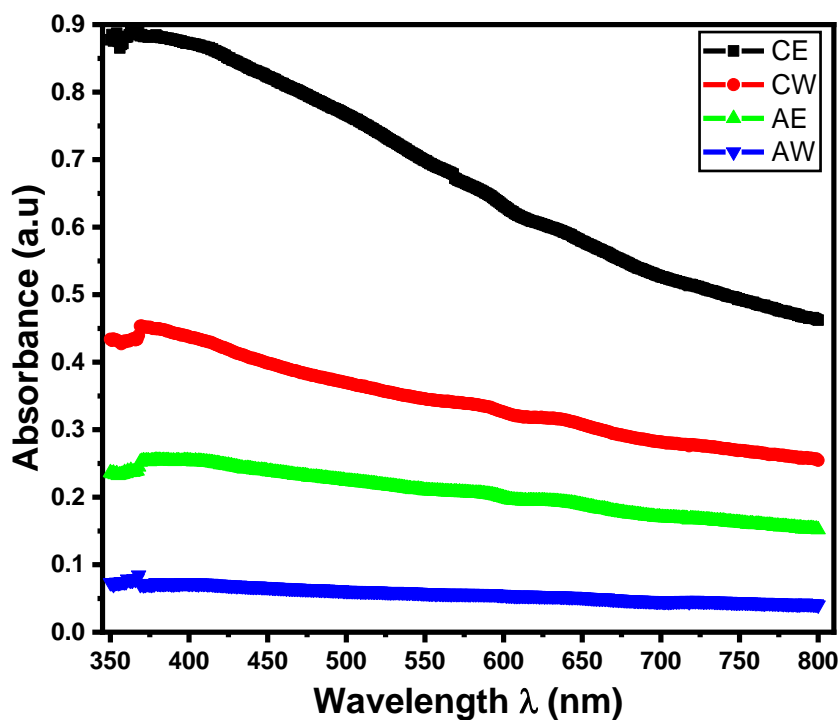


Fig. 3. Graph of absorbance versus wavelength for all the lone dyes

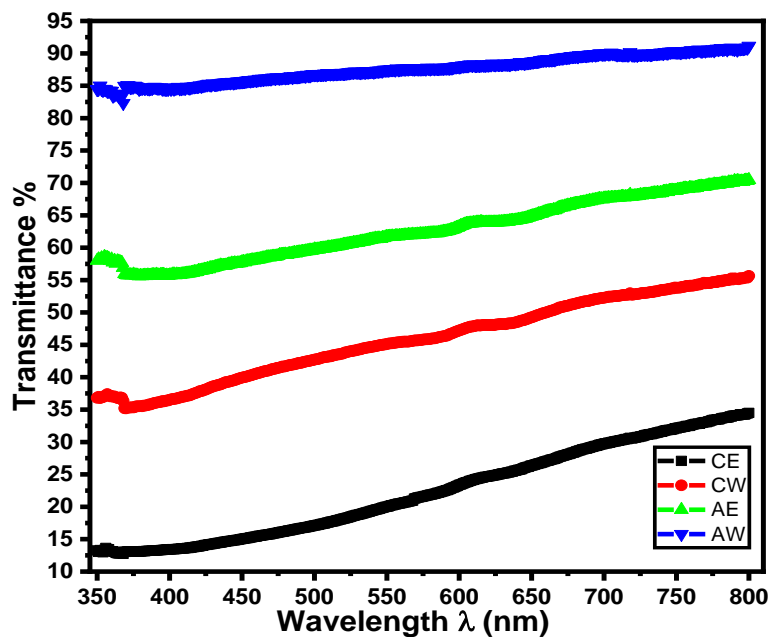


Fig. 4. Graph of transmittance versus wavelength for all the lone dyes.

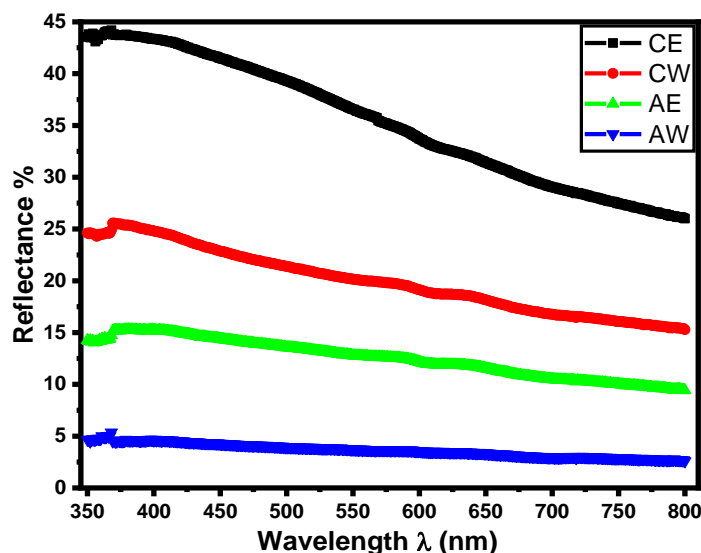


Fig. 5. Graph of reflectance versus wavelength for all the lone dyes.

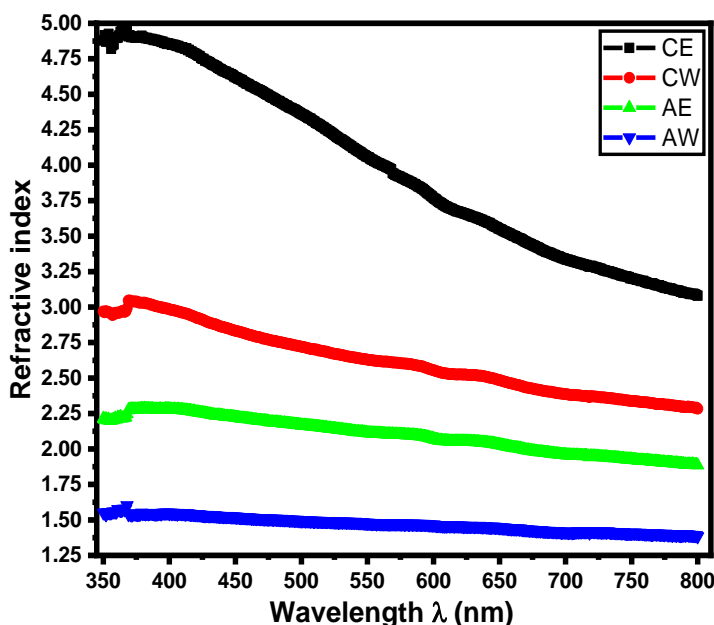


Fig. 6. Graph of refractive index versus wavelength for all the lone dyes

The graph of refractive index of the films as a function of wavelength for all the almond dyes is shown in Fig. 6. The refractive index of the films was calculated using the relationship as provided by (Onu et al., 2023; Achilefu et al., 2024; Muomeliri et al., 2024).

$$n = \frac{1+\sqrt{R}}{1-\sqrt{R}} \quad 3$$

Where R represents the calculated reflectance of the films.

The figure showed that the fabricated films generally have high values of refractive index with the film CE having the highest value in the range of 3.12 to 4.87, while the film AW has the lowest value in the range 1.4 – 1.6 throughout the VIS region of electromagnetic spectrum. The films AE and CW have the intermediate values in the range of 1.9 – 2.29 and 2.3 – 3.05 respectively. The figure also showed that the refractive index of the films decreased with an increase in wavelength indicating lower values in

the NIR. The high values of refractive index possessed by the films of this nature position them for device application such as waveguide, optical fibre and solar cells.

Fig. 7 represents the plots of  $(\alpha h\nu)^2$  against photon energy for all the deposited dye-sensitized films to determine the direct bandgap energy of the films. The bandgap energy of the films estimated through the Tauc's relation as provided by (REF), (Nwori et al., 2021).

$$\alpha h\nu = \beta (h\nu - E_g)^n \quad 4$$

Where n is the band transition factor which has values 0.5 for direct allowed band transition, 2 for indirect band electronic transition, 1.5 for direct forbidden band transition and 3 for indirect forbidden band transition,  $\beta$  is a constant known as band trailing parameter, h is the plank

constant,  $\nu$  is the frequency and  $\alpha$  is the absorption coefficient. The absorption coefficient ( $\alpha$ ) for the films was calculated using the formula given by Srivastava et al., (2013).

$$\alpha = \frac{A}{\lambda} \quad 5$$

From the figure, the bandgap energy of the films as estimated through extrapolation of the straight-line portion of the curves on the photon energy axes at the points  $(\alpha h\nu)^2$  equals to zero showed that the films exhibited wide bandgap energy values. The obtained values of the bandgap energies are 2.5 eV for the film CE, 2.6 eV for CW, and 2.4 eV for the films AE and AW each. These are in the range of wide bandgap energies and are favourable for application in the device that required high temperature and fabrication of blue LEDs devices.

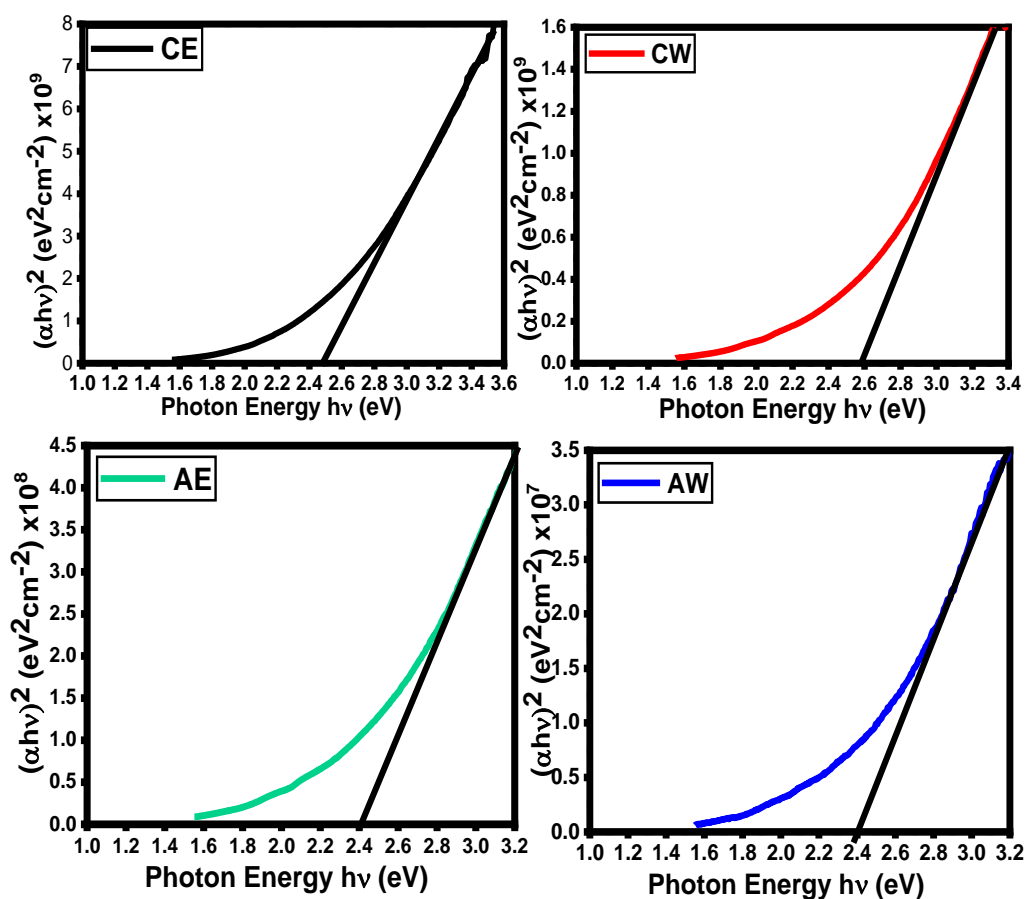


Fig. 7. Plots of  $(\alpha h\nu)^2$  versus photon energy for all the deposited lone dyes

### 3.2 Structural Properties of all the Deposited films

The XRD patterns of all the films deposited with almond leaf dyes treatment is presented in Fig. 8. The figure showed that the deposited films have crystalline structures with prominent sharp peak that occurred at two theta position 25.56° and other minor peaks as shown in the figure. The XRD patterns matched almost well with the standard JCPDS card numbers: 04-022-3337 for Anatase (TiO<sub>2</sub>) and 00-001-1081 for chalcocyanite (CuSO<sub>4</sub>). The average values of the crystallite size, micro-strain and dislocation density of the films calculated using Debye - Scherrer and Wilson relations are as shown in Table 1.

The crystallite size, micro-strain and dislocation density of the films were calculated using Debye - Scherrer and Wilson relations as provided by

(Jeroh & Okoli, 2012; Agobi et al., 2022; Talantikite-Touati et al., 2017; Mohamed, 2010).

$$D = \frac{0.9\lambda}{\beta \cos\theta} \quad 6$$

$$\delta = \frac{1}{D^2} \quad 7$$

$$\varepsilon = \frac{\beta}{4.T \tan\theta} \quad 8$$

### 3.3 Surface Morphological Properties of the Deposited Films

The surface micro-graph image of the deposited DSSCs films for all the almond leaf dyes under the treatment of alcohol and water is displayed in Fig. 9. The figure showed that the surface morphology of the film CE is highly smooth with no cracks or pores. However, the surface morphologies of the films CW, AE and AW are equally smooth but contain some cracks which act as trapping centre for photon absorptions.

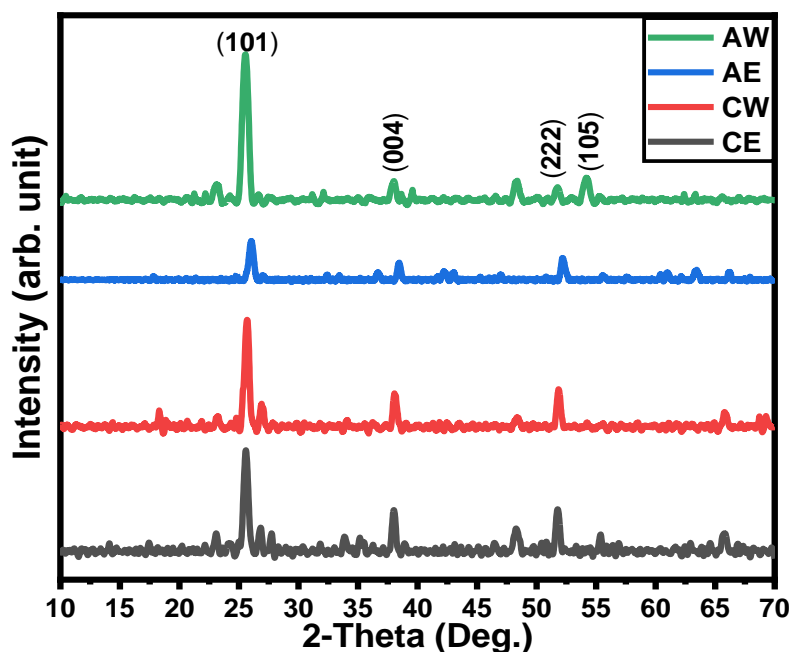
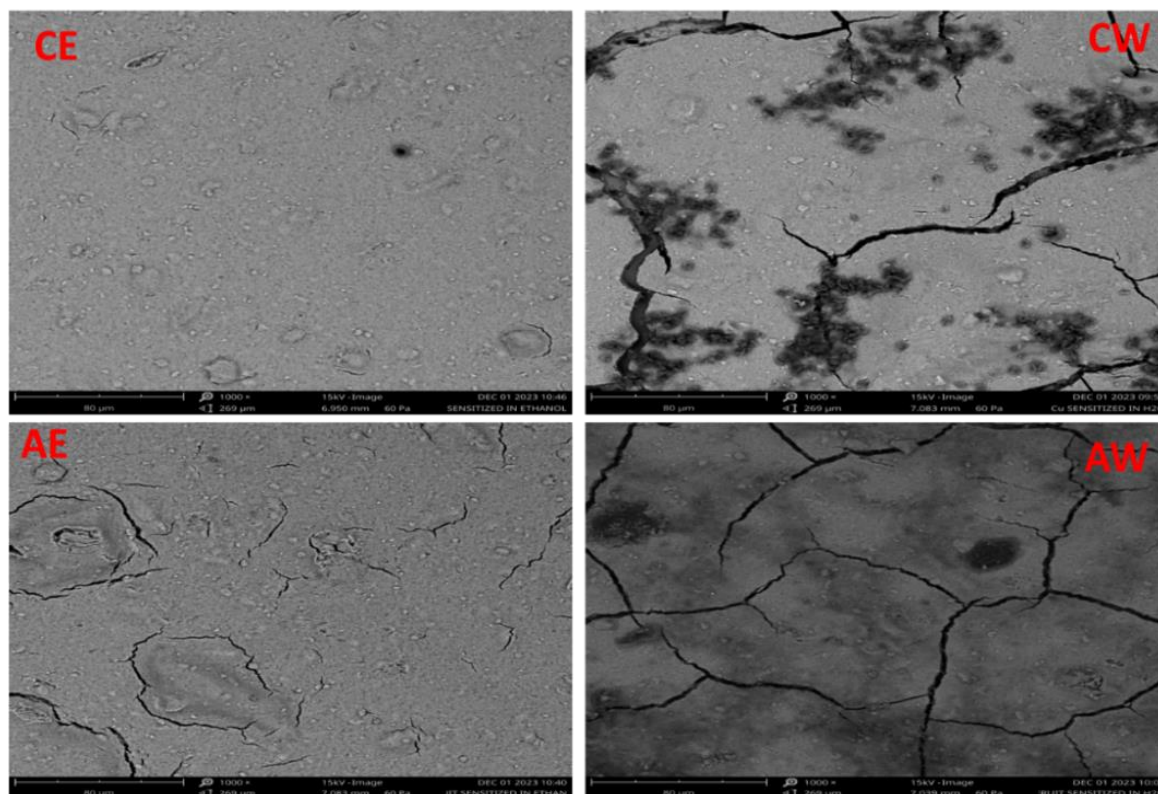


Fig. 8. X-ray diffraction pattern of the deposited DSSC for all the lone leaf dyes.

Table 1. Average values of the crystal parameters of the deposited DSSCs films

Samples	Crystallite Size (nm)	Micro-strain x10 <sup>-3</sup>	Dislocation Density (nm <sup>-2</sup> ) x10 <sup>-3</sup>
CE	24.55	4.23	1.96
CW	27.68	4.32	1.43
AE	22.27	11.99	3.18
AW	36.30	5.60	3.56



**Fig. 9. SEM micrograph of the fabricated DSSCs for all the lone leaf dyes**

### 3.4 I-V characteristic analysis of the Deposited Films

Fig. 10 is the current-voltage characteristic curves of the fabricated DSSCs for the lone almond and copper leaves extracted in ethanol and water. The curves were made and used to determine the various solar cell parameters of the deposited films for solar cell applications. The estimated values of the parameters which include  $V_{oc}$ ,  $V_{mp}$ ,  $J_{sc}$ ,  $J_{mp}$  of the films from the curve and calculated values of fill factor (FF) and cell efficiency are presented in Table 2. The fill factor and cell efficiency were calculated using the relations as provided by

(Ezenwaka et al., 2022; Emmanuel et al., 2022; Keita et al., 2023).

$$ff = \frac{I_{mp}V_{mp}}{I_{sc}V_{oc}} \quad 9$$

$$Cell\ efficiency\ (\eta) = \left(\frac{I_{sc}V_{oc}}{P_{in}} \cdot ff\right)100\% \quad 10$$

Where  $P_{in}$  is the solar illumination intensity used. From the Table 2, it can be observed that the cell efficiency of both the lone dye sensitized films is very low. The low conversion efficiency exhibited by films can be attributed to the film quality and structures with a record low efficiency for the dye-sensitized films very close to this work reported by (Baba Alfa et al., 2012).

**Table 2. Summary of the PV parameters and performance of the I-V Curves**

Samples	$V_{oc}$ (V)	$V_{mp}$ (V)	$I_{sc}$ (mA)	$I_{mp}$ (mA)	FF	Efficiency $\eta$ (%)
AE	0.44	0.25	0.076	0.051	0.381	0.0013
AW	0.47	0.27	0.45	0.311	0.397	0.0088
CE	0.48	0.32	0.135	0.1	0.493	0.0033
CW	0.48	0.33	0.116	0.09	0.533	0.0031

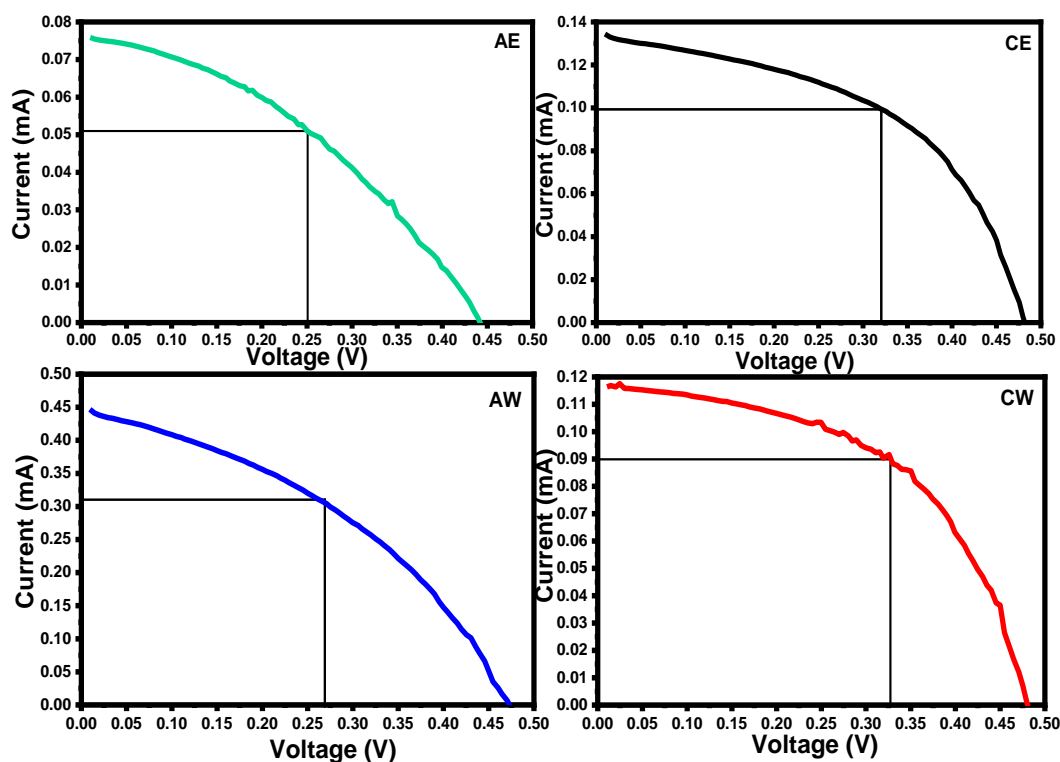


Fig. 10. I-V curves of the almond and copper leaves in ethanol and water DSSCs films

#### 4. CONCLUSION

The dye-sensitized solar cells (DSSCs) thin film structures of TiO<sub>2</sub> deposited on FTO glass substrate using the method of Dr. Blading have been successfully synthesized in this work for possible applications. The dyes of almond leaf (*terminali catappa*), copper leaf (*acalypha wilkesiana*) extracted using ethanol and water were used as photo-sensitizer on the deposited films to determine their separate effects on the TiO<sub>2</sub> for their applications. The deposited films were subjected to different characterisations to determine their characteristic features suitable for applications. The optical analysis carried out on the films showed that absorbance of the lone copper leaf dyes-sensitized films is higher than that of the almond leaf dye-sensitized films. All the deposited films have high values of refractive index throughout the VIS region. The deposited films have wide bandgap energy values with the values 2.5 eV for the film CE, 2.6 eV for CW, and 2.4 eV for the films AE and AW each. These values position the DSSCs films for many applications including high temperature and fabrication of blue LEDs devices. The structural analysis revealed that the deposited films are crystalline in nature with acceptable strain level

thereby positioning the material for solar cell matrix fabrication for solar energy harnessing.

#### DISCLAIMER (ARTIFICIAL INTELLIGENCE)

Author(s) hereby declare that NO generative AI technologies such as Large Language Models (ChatGPT, COPILOT, etc) and text-to-image generators have been used during writing or editing of this manuscript.

#### COMPETING INTERESTS

Authors have declared that no competing interests exist.

#### REFERENCES

- Achilefu B. C, Okpala U. V & Nwori A. N (2024). Influence of Walnut Shell Dopant on the Properties of Walnut Doped-PbS Thin Film Crystals Grown by Sol-gel Technique. International Journal of Scientific Research in Physics and Applied Sciences, 12(2), 0-17.
- Agobi, A. U., Ekpunobi, A. J., Ikeuba, A. I., Ikhioya, I. L., Ozoemena, C. N., & Udofia, K. I. (2022). Hybrid

- polypyrrole/copper/graphene oxide nanocomposite films synthesized via potentiostatic deposition with enhanced photovoltaic properties. *Journal of the Indian Chemical Society*, 99(7), 100549.
- Baba Alfa, Matthew Tersoo Tsepav, Raymond Limen Njinga, Ibrahim Abdulrauf (2012). Fabrication and Characterisation of Titanium Dioxide Based Dye Sensitized Solar Cell using Flame of the Forest Dye. *Applied Physics Research*, 4(1), 48-56.
- Chou, T. P., Zhang, Q., & Cao, G. (2007). Effects of dye loading conditions on the energy conversion efficiency of ZnO and TiO<sub>2</sub> dye-sensitized solar cells. *The Journal of Physical Chemistry C*, 111(50), 18804-18811.
- Emmanuel, O. C., Donald, O. N., & Ikhioya, I. L. (2022). Effect of Doping and Co-sensitization on the Photovoltaic Properties of Natural Dye-sensitized Solar Cells. *SSRG International Journal of Applied Physics*, 9(3), 44-54.
- Ezenwaka, L. N., Nwori, A. N., Ottih, I. E., Okereke, N. A., & Okoli, N. L. (2022). Investigation of the optical, structural and compositional properties of electrodeposited lead manganese sulfide (PbMnS) thin films for possible device applications. *Nanoarchitectonics*, 18-32.
- Ezenwaka, L. N., Okoli, N. L., Okereke, N. A., Ezenwa, I. A., & Nwori, N. A. (2022). Properties of electrosynthesized cobalt doped zinc selenide thin films deposited at varying time. *Nanoarchitectonics*, 1-17.
- Grant, C. D., Schwartzberg, A. M., Smestad, G. P., Kowalik, J., Tolbert, L. M., & Zhang, J. Z. (2002). Characterization of nanocrystalline and thin film TiO<sub>2</sub> solar cells with poly (3-undecyl-2, 2'-bithiophene) as a sensitizer and hole conductor. *Journal of electroanalytical Chemistry*, 522(1), 40-48.
- Hatem S. El-ghamri, Taher M. El-agezi, Sofyan A. Tayal, Amal Y. Batnijii (2014). "Dye-sensitized solar cells with natural dyes extracted from plant seeds. *Materials Science-Poland*, 32(4), 547-554.
- Jeroh, M. D., & Okoli, D. N. (2012). Optical and structural properties of amorphous antimony sulphide thin films: Effect of dip time. *Adv. Appl. Sci. Res*, 3(2), 793-800.
- Keita, E. H. M, Mbaye, F., Dia, M., Sow, C., Sene, C., & Mbow, B. (2023). Real Solar Cell and Determination Methods of Electrical Parameters. *OAJ Materials and Devices*, 7, 1-12.
- Mehmood, U., Aslam, M. Z., Shawabkeh, R. A., Hussein, I. A., Ahmad, W., & Rana, A. G. (2016). Improvement in photovoltaic performance of dye sensitized solar cell using activated carbon-TiO<sub>2</sub> composites-based photoanode. *IEEE journal of photovoltaics*, 6(5), 1191-1195.
- Mehmood, U., Rahman, S., Harrabi, K., Hussein, I.A. and Reddy, B.V.S (2014). Recent Advances in Dye Sensitized Solar Cells. *Journal of Advances in Materials Science and Engineering*, 6, 578-594.
- Millington, K.R (2009). Dye-sensitized cells," in *Encyclopedia of Electrochemical PowerSources*, 10–21.
- Mohamed, S. H. (2010). Photocatalytic, optical and electrical properties of copper-doped zinc sulfide thin films. *Journal of physics D: applied physics*, 43(3), 1-8.
- Muomeliri, C. B., Ekpunobi, A. J., Okoli, D. N., Azubogu A. C., Nwori A. N., Mimi J. D., Anusiuba O. I., Okafor C. E, Ozobialu L & Nwaodo, A., (2024). Effects of Deposition Periods on the Optical and Structural Properties of Electrochemically Deposited Nickel-Doped Zinc Oxide Thin Films. *Journal of Physics and Chemistry of Materials*, 11(3), 01-10.
- Nwokoye, A. O. C., & Okoye, I. F. (2020). Profilometry Analysis of Fluorine Doped Tin Oxide (FTO) Film Mesoporous (M-TiO<sub>2</sub>) Film Using Organic Dye from Senna Plant as a Photosensitizer. *Der Chemica Sinica*, 11, 1-6.
- Nwori, A. N., Ezenwaka, N. L., Ottih, I. E., Ngozi, A. O., & Okoli, N. L. (2021). Study of the Optical, Electrical, Structural and Morphological Properties of Electrodeposited Lead Manganese Sulphide (PbMnS) Thin Film Semiconductors for Possible Device Applications. *Journal of Modern Materials*, 8(1), 40-51.
- Nwori, A. N., Okoli, N. L., Okereke, N. A., Ottih, I. E., & Ezenwaka, L. N. (2022). Optical Properties of Electrodeposited CdMnS Thin Film Semiconductor Alloys for Optoelectronics Applications: Effect of Deposition Potential. *Journal of Nano and Materials Science Research*, 1, 58-67.
- Okereke, N. A., & Ekpunobi, A. J. (2011). ZnSe buffer layer deposition for solar cell application. *Journal of Non-oxide glasses*, 3(1), 31-36.
- Onu, C. P., Ekpunobi, A. J., Okafor, C. E., & Ozobialu, L. A. (2023). Optical properties of monazite nanoparticles prepared via ball

- millling. *Asian Journal of Research and Reviews in Physics*, 7(4), 17-29.
- O'regan, B., & Grätzel, M. (1991). A low-cost, high-efficiency solar cell based on dye-sensitized colloidal TiO<sub>2</sub> films. *nature*, 353(6346), 737-740.
- Qin, Y., & Peng, Q. (2012). Ruthenium sensitizers and their applications in dye-sensitized solar cells. *International Journal of Photoenergy*, 2012(1), 291579.
- Srivastava, M., Singh, J., Mishra, R. K., & Ojha, A. K. (2013). *Electro-optical and magnetic properties of monodispersed colloidal Cu<sub>2</sub>O nanoparticles*. *Journal of Alloys and Compounds*, 555, 123–130. Doi:10.1016/j.jallcom.2012.12.049
- Talantikite-Touati, D., Merzouk, H., Haddad, H., & Tounsi, A. (2017). Effect of dopant concentration on structural and optical properties Mn doped ZnS films prepared by CBD method. *Optik*, 136, 362-367.
- Tennakone, K., Kumara, G. R. R. A., Kumarasinghe, A. R., Wijayantha, K. G. U., & Sirimanne, P. M. (1995). A dye-sensitized nano-porous solid-state photovoltaic cell. *Semiconductor Science and Technology*, 10(12), 1689.
- Tsokos, K. A. (2008). *Physics for the IB Diploma*. Cambridge University Press.
- Zhang, G., Bala, H., Cheng, Y., Shi, D., Lv, X., Yu, Q., & Wang, P. (2009). High efficiency and stable dye-sensitized solar cells with an organic chromophore featuring a binary  $\pi$ -conjugated spacer. *Chemical Communications*, (16), 2198-2200.

**Disclaimer/Publisher's Note:** The statements, opinions and data contained in all publications are solely those of the individual author(s) and contributor(s) and not of the publisher and/or the editor(s). This publisher and/or the editor(s) disclaim responsibility for any injury to people or property resulting from any ideas, methods, instructions or products referred to in the content.

© Copyright (2024): Author(s). The licensee is the journal publisher. This is an Open Access article distributed under the terms of the Creative Commons Attribution License (<http://creativecommons.org/licenses/by/4.0>), which permits unrestricted use, distribution, and reproduction in any medium, provided the original work is properly cited.

Peer-review history:  
The peer review history for this paper can be accessed here:  
<https://www.sdiarticle5.com/review-history/127155>